

Microstructure and mechanical behaviour of 3Y–TZP/Mo nanocomposites possessing a novel interpenetrated intragranular microstructure

M. NAWA, K. YAMAZAKI

Central Research Laboratory, Matsushita Electric Works, Ltd., 1048, Kadoma, Osaka 571, Japan

T. SEKINO, K. NIIHARA

The Institute of Scientific and Industrial Research, Osaka University, 8-1, Mihogaoka, Ibaraki, Osaka 567, Japan

Yttria stabilized tetragonal zirconia polycrystal (Y–TZP)/0–100 vol% molybdenum (Mo) composites were fabricated by hot-pressing a mixture of Y–TZP powder containing 3 mol % yttria (Y_2O_3) and a fine Mo powder in vacuum. This composite system possessed a novel microstructural feature composed of an interpenetrated intragranular nanostructure, in which either nanometer sized Mo particles or equivalent sized zirconia (ZrO_2) particles located within the ZrO_2 grains or Mo grains, respectively. The strength and toughness were both greatly enhanced with increasing Mo content for the 3Y–TZP/Mo composites thus breaking through the strength–toughness tradeoff relation in transformation toughened ZrO_2 and its composite materials. They exhibited a maximum strength of 2100 MPa and a toughness of $11.4 \text{ MPa}\cdot\text{m}^{1/2}$ for the composite containing 70 vol % Mo. These simultaneous improvements in strength and toughness were determined to be the result of a decrease in flaw size associated with the interpenetrated intragranular nanostructure, and a stress shielding effect created in the crack tip by the elongated Mo polycrystals bridging the crack tip in addition to the stress induced phase transformation.

1. Introduction

Ceramics are currently being investigated as candidates for a wide variety of engineering applications due to their desirable properties such as high refractory capability, good wear resistance, and chemical stability. However, they have not yet found any significant applications due mainly to their poor toughness. Therefore, it is highly desirable to improve the reliability of ceramics, which possesses high tolerance for catastrophic fracture.

Of particular interest are tetragonal zirconia polycrystals (TZP), stabilized with Y_2O_3 (Y–TZP) or CeO_2 (Ce–TZP), since they show either a high strength or a high toughness [1–3]. However, it is apparent that the attractive property of the TZP ceramic and TZP based composites is accompanied by either a modest toughness for the Y–TZP system or a modest strength for the Ce–TZP system. For example, Y–TZP ceramics containing 2 to 3 mol % Y_2O_3 have exhibited enhanced strength values above 1200 MPa even under pressureless sintering. In addition, Y–TZP based composites containing 30 vol % Al_2O_3 , after isostatically hot-pressing, have shown a significant improvement in strength to 2400–3000 MPa [4,5]. However, these Y–TZP ceramics have toughness values in the range of $5\text{--}6 \text{ MPa}\cdot\text{m}^{1/2}$ [2].

On the other hand, Ce–TZP ceramics containing 7–12 mol % CeO_2 have exhibited fairly high toughness values of $10\text{--}20 \text{ MPa}\cdot\text{m}^{1/2}$ [3], but show, strength values of only 600–800 MPa. In Ce–TZP based composites containing 50 vol % Al_2O_3 , the toughness values decreased remarkably from 20 to $5.5 \text{ MPa}\cdot\text{m}^{1/2}$ with increasing Al_2O_3 content, in contrast to the slight improvement in strength to 900 MPa [6]. Thus, the tradeoff relation between high strength and high toughness is still unresolved for both types of monolithic TZP and TZP/ Al_2O_3 composite systems.

For the strength–toughness relationship, Swain *et al.* [7] proposed a mechanism for the limitation of strength in transformation toughened zirconia. They pointed out that the maximum strength is limited by the critical stress that induces the tetragonal-to-monoclinic transformation. The strength is then controlled by the inherent R-curve behaviour due to the martensitic transformation. Thus, for transformation toughened zirconia with a constant inherent flaw size, the strength increases with increasing toughness, however, the strength reaches a maximum value when it is equal to the critical transformation stress and then decreases with further increasing toughness. According to this hypothesis, it seems to be extremely difficult

to improve both strength and toughness simultaneously in transformation toughened zirconia and its composite systems.

To overcome the strength-toughness tradeoff relation in the Y-TZP based composite system, we have investigated another approach to preserving high strengths up to the region of high toughness. In this study, ductile refractory metal particles have been prepared as secondary dispersions. In this system, it is expected that the metal phase will result in the inherent improvement of toughness. However, most ceramic matrix composites incorporating metal dispersions such as tungsten (W), molybdenum (Mo), titanium (Ti), chromium (Cr), nickel (Ni), etc. [8-13] do not always produce successful results. This is mainly due to the fact that the addition of micrometer sized second phase dispersions generally causes an enlargement of the flaw size in the composites. Therefore, it is a serious point of contention whether or not the flaw size can be decreased and/or restrained successfully in order to simultaneously improve both strength and toughness.

In recent years, nanocomposites, in which nanometer sized second ceramic particles are dispersed within the ceramic matrix grains and/or at the grain boundaries, have been investigated in an attempt to eliminate the strength-degrading flaws [14,15]. They have shown significant improvements in strength and creep resistance even at high temperatures. However, the enhancement of toughness was still modest in comparison with that of other conventional ceramic composites. In previous work, in order to further improve the toughness of ceramic based nanocomposites, we applied the idea of nanocomposites to ceramic/metal systems. In $\text{Al}_2\text{O}_3/\text{Mo}$ composites, we succeeded in fabricating ceramic/metal nanocomposites containing nanometer sized Mo particles within the Al_2O_3 grains and/or at the grain boundaries [16]. They showed a fair improvement in strength resulting from the fine-grained microstructure associated with the existence of nanometer sized Mo particles. However, the nanometer sized Mo particles within the Al_2O_3 grains and/or at the grain boundaries exhibited little effect towards improving the toughness. Instead, we determined a possible method of inherent improvement in the toughness, due to the relaxation of the stress intensity by the coalescence of elongated Mo particles combining at the Al_2O_3 grain boundaries, although the strength decreased in the high toughness region.

In this study, we have extended the results of the $\text{Al}_2\text{O}_3/\text{Mo}$ nanocomposites to the Y-TZP/Mo composite system and have succeeded in achieving a simultaneous improvement in the strength and toughness thereby overcoming the strength-toughness tradeoff relation [17]. In this paper, the microstructural features for Y-TZP/0-100 vol % Mo composites and the relationship between their mechanical properties will be discussed.

2. Experimental procedure

2.1. Fabrication

Y-TZP powder containing 3 mol % Y_2O_3 (grade TZ-3Y, Tosoh Co., Tokyo, Japan) was used as the

ceramic matrix and Mo powder (grade Mo-H-D, Japan New Metals Co., Osaka, Japan) was selected for the metal dispersions. The average grain size of the 3Y-TZP and Mo powder were 0.2 μm and 0.65 μm , respectively. Moreover, the Mo powder had a bimodal particle size distribution with two peaks at 0.2 μm and 1.2 μm . The powder mixtures, containing 10, 20, 30, 40, 50, 60, 70, 80 and 100 vol % Mo, were ball milled using a zirconia milling media in acetone for 24 h. The slurries were dried and passed through a 250 μm screen. Then the mixtures were hot-pressed in carbon dies of 46 mm diameter. The hot-pressing conditions were 1400, 1500 and 1600 $^\circ\text{C}$ with an applied pressure of 30 MPa for 1 h in vacuum of less than 1.33×10^{-2} Pa.

2.2. Characterizations

The densities of the specimens were obtained by the Archimedes method using a toluene medium. Phase identifications of the composites were determined on the polished surfaces of the specimens by X-ray diffraction (XRD) analysis with $\text{CuK}\alpha$ radiation. The tetragonal, monoclinic and cubic phases were evaluated using the analysis of Garvie and Nicholson [18] and the volume fraction of the monoclinic phase was determined using the equation of Toraya *et al.* [19]. Furthermore, residual stress on the polished surface of the specimen was measured for 3Y-TZP/Mo composites containing 0, 10, 20, 30, 40, 50, 80 and 100 vol % Mo. The residual stresses of the ZrO_2 and Mo phases were determined on the diffraction planes of tetragonal ZrO_2 (312) and Mo (310) with $\text{FeK}\alpha$ radiation, and were calculated by the iso-inclination technique of the $\sin^2\psi$ method. The incident beam of the X-ray (ψ) is 0° and changed at 5° intervals from 10° - 45° . Poisson's ratio of each composite was calculated assuming that it obeys the rule of mixtures, where the Poisson's ratio of ZrO_2 and Mo are 0.310 [20] and 0.324 [21], respectively. The value of the elastic modulus used was measured in these studies. Lattice constants of the tetragonal ZrO_2 phase for 3Y-TZP/Mo composites, containing 0, 30 and 50 vol % Mo, were determined by X-ray diffraction analysis with $\text{CrK}\alpha$ radiation based on the outer standard method using Si powder. Finally, the microstructure of the composites was observed by scanning electron microscopy (SEM) and transmission electron microscopy (TEM).

2.3. Mechanical properties

The hot-pressed specimens were cut by a diamond blade saw, and ground with a 600-grit diamond wheel. The specimens, having dimensions of $3 \times 4 \times 40$ mm, were subjected to the elastic modulus measurement and the mechanical properties test. The elastic modulus was determined by the resonance vibration method with first-mode resonance. The fracture strength was measured by a three-point bending test at room temperature. The span length and cross head speed were 30 mm and 0.5 mm min^{-1} , respectively. The tensile surfaces of the specimens were perpendicular

to the hot-pressing axis and were polished with a diamond liquid suspension. The fracture toughness was estimated by the indentation–fracture (IF) method using the following equation of Marshall & Evans [22].

$$K_{IC} = 0.036E^{0.4}P^{0.6}a^{-0.7}(c/a)^{-1.5} \quad (1)$$

Where E is the elastic modulus and P is an applied load. Here a and c are characteristic dimensions of the Vickers impression and the radial/median crack, respectively. The polished surfaces were used for the Vickers indentation with a load of 196 N and a loading duration of 15 s. The Vickers hardness was also calculated from the result of the IF method. Separately, the toughness was also estimated by the single edge V notched beam (SEVNB) method. The V notch was machined using a special diamond slicing wheel, which was developed by Awaji *et al.* [23]. The half size V notched specimens, having dimensions of $3 \times 4 \times 20$ mm, were subjected to a 3-point bending test with a span length of 16 mm and a cross head speed of 0.5 mm min^{-1} . The value of toughness was calculated by using the Srawley shape coefficient [24].

3. Results and discussion

3.1. Microstructure

Relative densities higher than 99.5 % were obtained for the composites containing up to 100 vol % Mo hot-pressed at 1400–1600 °C. On the basis of the X-ray diffraction analysis, 3Y–TZP/Mo composites containing 10–80 vol % Mo were composed of only ZrO_2 and Mo. No crystalline reaction phases were detected. The ZrO_2 matrix in these 3Y–TZP/Mo composites consisted primarily of the tetragonal phase and a small amount (less than 7.5 vol %) of the monoclinic phase. There were no traces of the cubic phase.

The variations of microstructure with Mo content for the 3Y–TZP/Mo composites, containing 10–60 vol % Mo, are shown in Fig. 1. The microstructures of the composites were characterized by SEM using polished surfaces that were thermally etched in Argon at 1450 °C for 30 min. In the low concentration range (less than 30 vol %) of Mo content, it was recognized that submicron sized Mo particles were dispersed at the grain boundaries of the fine-grained/submicron sized ZrO_2 grains. On the other hand, with increasing Mo content, up to 30 vol %, slight grain growth of Mo particles was observed. In addition, in the range above 40 vol % Mo, the formation of elongated Mo polycrystals, which were formed due to the necking of Mo particles, was observed at the ZrO_2 grain boundaries. Finally, for above 60 vol % Mo content, a linked structure of Mo layers, which was interconnected with ZrO_2 grains, was produced. In contrast to the variation of Mo particles, the grain sizes of the ZrO_2 matrix were little influenced by the Mo content. That is, the ZrO_2 matrix was maintained as a fine-grained/submicron sized microstructure for all Mo content values. Furthermore, in the range from 30–50 vol % Mo, a number of ultra-fine Mo particles were preferentially dispersed within the ZrO_2 grains

and at the grain boundaries, which were located next to the elongated Mo polycrystals.

A TEM image of the 3Y–TZP/40 vol % Mo composite hot-pressed at 1600 °C is shown in Fig. 2. It was recognized that a novel interpenetrated intragranular microstructure was present in the 3Y–TZP/Mo composite, in which either nanometer sized Mo particles or isolated equivalent sized ZrO_2 particles were trapped within the ZrO_2 grains or Mo grains, respectively. Furthermore, the existence of extremely fine Mo particles within the ZrO_2 grain was also identified. The isolated ultra-fine Mo particles of less than 10 nm diameter within the ZrO_2 grain are shown in Fig. 3. In addition, a similar microstructural feature, that was recognized in the 3Y–TZP/70 vol % Mo composite, is shown in Fig. 4. In this case, however, the ultra-fine Mo particles within the ZrO_2 grain were oriented to the preferred crystal direction. This orientation of the ultra-fine Mo particles was determined to be correlated in a coherent alignment with the crystal direction of the ZrO_2 grain. A TEM image of the monolithic Mo hot-pressed at 1600 °C is shown in Fig. 5. Unexpected secondary phases (white particles) were observed within the Mo grains and at the grain boundaries. By examination of the energy dispersive X-ray analysis (EDAX) data, the white grains were ascertained to contain large amounts of oxygen in contrast to the Mo grains. In addition, on the basis of the X-ray diffraction analysis, the MoO_2 phase was detected in small concentrations. Therefore, it was concluded that the secondary phase was MoO_2 , which was probably formed by the oxidation by oxygen and/or hydroxyl groups absorbed around the surfaces of the starting Mo powders. In addition, the MoO_2 phase was only detected in the monolithic Mo. As will be described below, this phenomenon helps to understand the formation mechanism of the ultra-fine Mo particles within the ZrO_2 grains.

The lattice constant and the axial ratio of the tetragonal ZrO_2 , for the monolithic and the 3Y–TZP/Mo composites containing 30 and 50 vol % Mo, are presented in Table I. It was shown that the lattice constants of the tetragonal ZrO_2 phase decreased with increasing Mo content and the axial ratio increased with increasing Mo content. These results suggest that a molybdenum ion such as Mo^{4+} and/or Mo^{6+} , having a smaller ionic radius than those of Y^{3+} and/or Zr^{4+} , was present in the tetragonal ZrO_2 lattice, although the exact configuration of this solid solution is not clear. The inference here, is probably that, the molybdenum ion forms either an interstitial solid solution in the site of the eightfold coordination of Zr^{4+} or a substitutional solid solution in the site of Y^{3+} . Here, judging from the result that the MoO_2 phase was only detected in the monolithic Mo, it is assumed that the MoO_2 phase would provide a molybdenum ion such as Mo^{4+} . Anyhow, the ultra-fine Mo particles are supposed to be *in situ* precipitated from a supersaturated solid solution of ZrO_2 during the cooling process in the hot-pressing procedure. The argument remains, however, that such tiny Mo particles might be oxidized into various valence levels such as those found in Mo_9O_{26} , Mo_4O_{11} and MoO_2 .

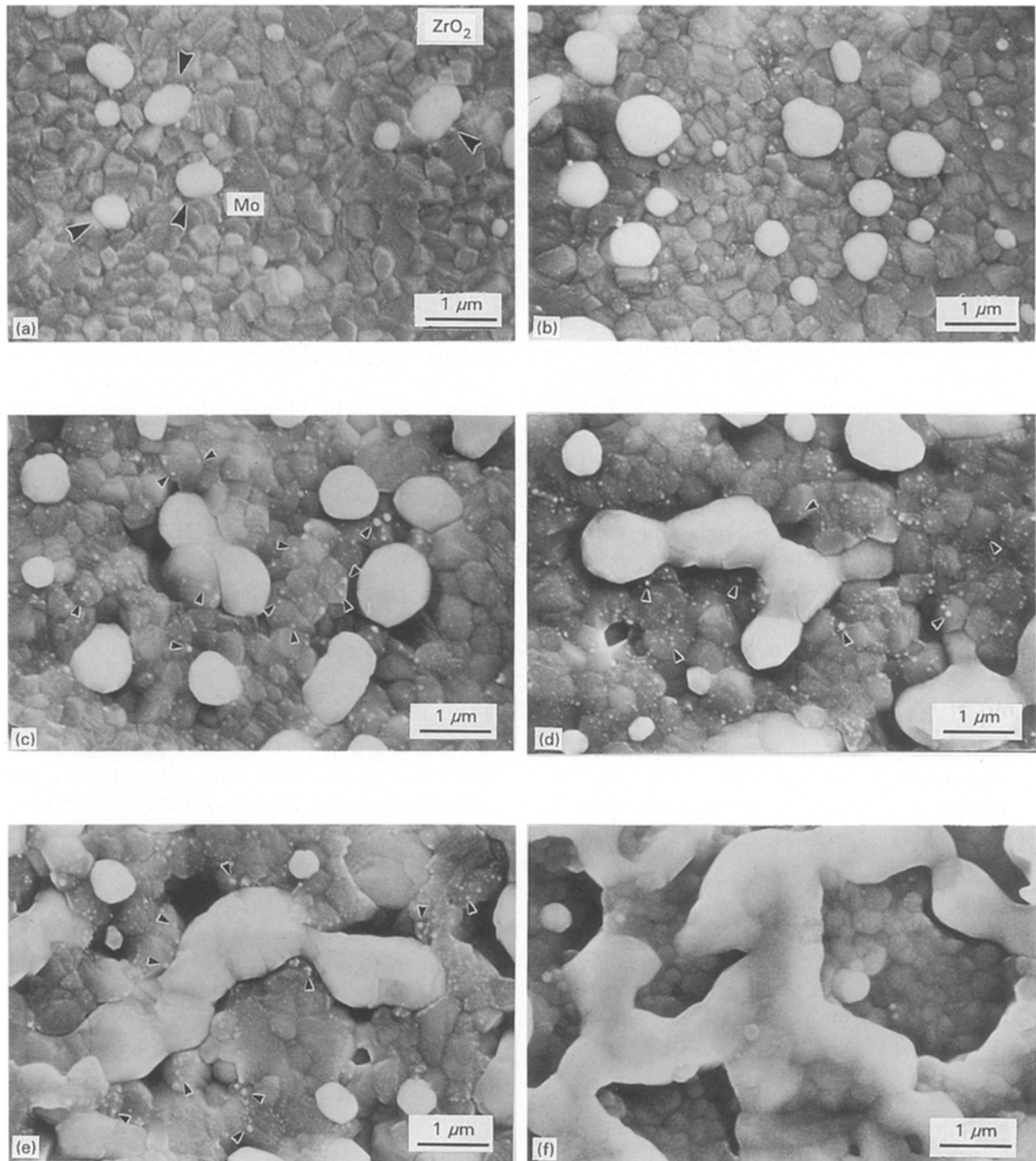


Figure 1 SEM photographs of thermal-etched surfaces for 3Y-TZP/Mo composites hot-pressed at 1500°C containing 10 vol % (a), 20 vol % (b), 30 vol % (c), 40 vol % (d), 50 vol % (e) 60 vol % (f) Mo.

The interface between the ZrO₂ and the Mo grain boundaries for the 3Y-TZP/40 vol % Mo composite is shown in Fig. 6. Twins were observed in the ZrO₂ grain next to the large Mo particle, which were caused from the tetragonal-to-monoclinic transformation. As shown in Fig. 7, dislocation lines were also observed around the nanometer sized Mo particle within the ZrO₂ grain. X-ray residual stress studies of both ZrO₂ and Mo phases, as a function of Mo content for the 3Y-TZP/Mo composites, is shown in Fig. 8. It was ascertained that the residual stress of the ZrO₂ phase approximately tended to increase on the tensile side and that of the Mo decreased on the compression side

with increasing Mo content. This overall variation of residual stresses with Mo content was generally in good agreement with the predicted relation, which is estimated by their thermal expansion mismatch. However, the inflection points were observed in each ZrO₂ and Mo phases at around 30–50 vol % Mo content. This variation is currently not well understood, however, this seems to be correlated to the formation of the ultra-fine Mo particles within the ZrO₂ grains. Consequently, it seems reasonable to assume that the localized internal stresses within the ZrO₂ grains and/or around the Mo particles exist in the 3Y-TZP/Mo composites.

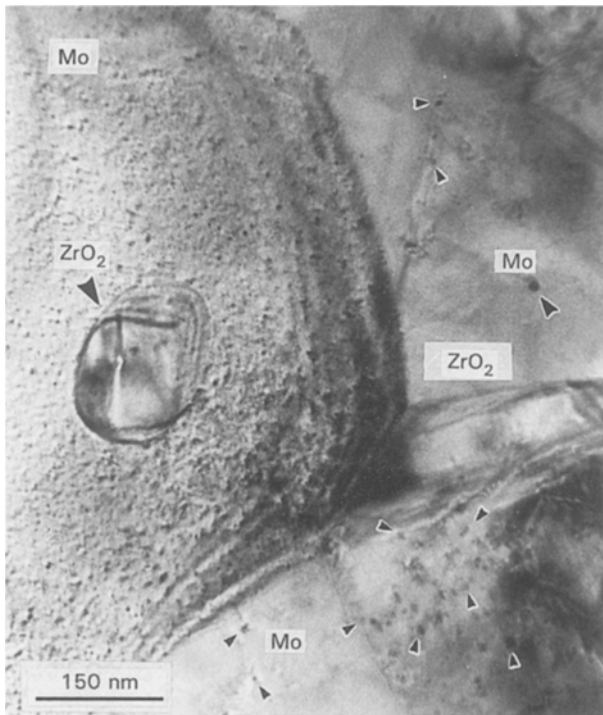


Figure 2 TEM image of an interpenetrated intragranular microstructure for 3Y-TZP/40 vol % Mo composite hot-pressed at 1600 °C.

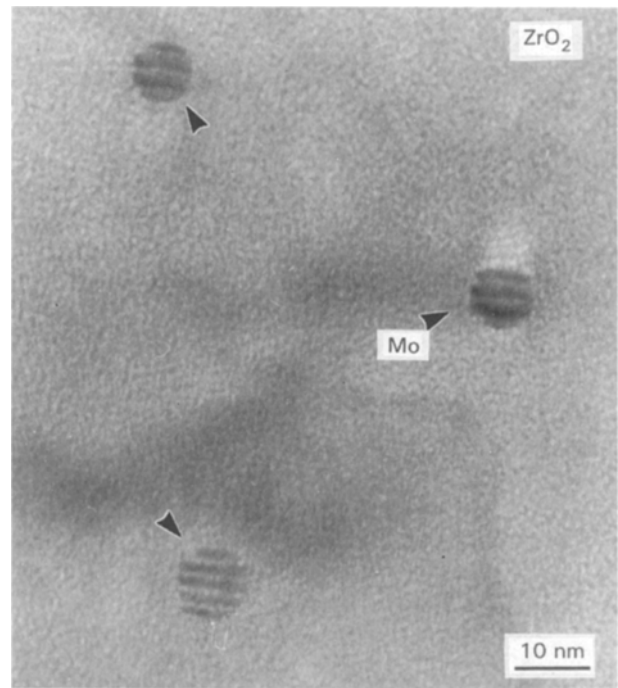


Figure 4 A similar microstructural feature associated with ultra fine Mo particles within the ZrO₂ grain for 3Y-TZP/70 vol % Mo composite hot-pressed at 1600 °C.

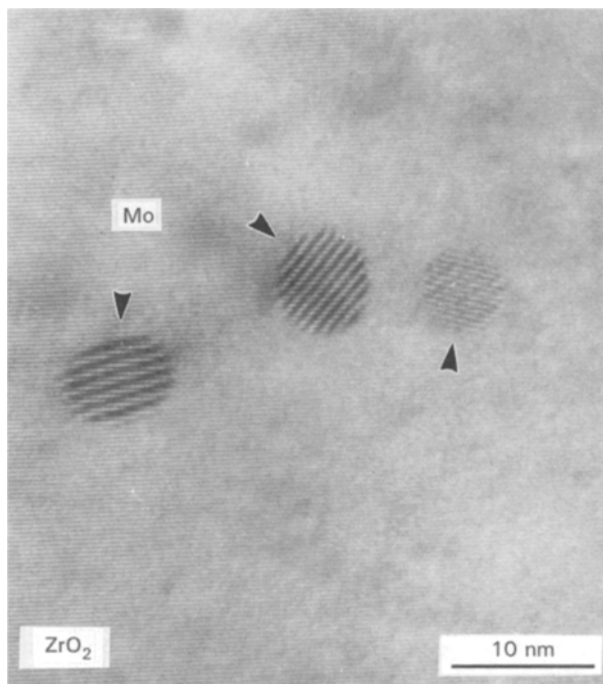


Figure 3 High-resolution TEM image of the ultra fine Mo particles of less than 10 nm observed within the ZrO₂ grain.

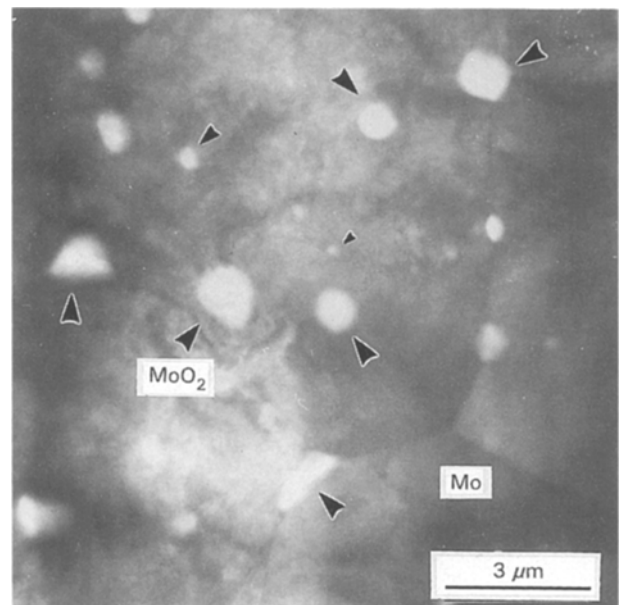


Figure 5 TEM image of the microstructure of the monolithic Mo hot-pressed at 1600 °C.

3.2. Mechanical properties

The fracture strength as a function of Mo content for the 3Y-TZP/0–100 vol % Mo composites is shown in Fig. 9. The strength increased with increasing Mo content up to 50 vol % and obtained a semi-maximum value of 1795 MPa for the 3Y-TZP/40 vol % Mo composite hot-pressed at 1600 °C. Then, a steep increase in the strength was observed in the range

from 50–70 vol % Mo content. A maximum value of 2100 MPa was obtained for the 3Y-TZP/70 vol % Mo composite hot-pressed at 1500 °C. This strengthening was determined to be the result of two separate phenomena. The first concerns a decrease in a flaw size for both the ZrO₂ and the Mo grains, respectively, associated with the interpenetrated intragranular microstructure. That is, nanometer sized inclusions, which are trapped inside the grain, are believed to have a role in dividing a grain into more finer sized particles. In particular, for the composites containing above 50 vol % Mo content, the strengthening is derived from the modification of

TABLE I Lattice constant and axial ratio of tetragonal ZrO_2 for 3Y-TZP/Mo composites hot-pressed at 1500 °C containing 0, 30 and 50 vol % Mo.

	$a, b \times 10^{-1}$ (nm)	$c \times 10^{-1}$ (nm)	$c/\sqrt{2a}$	volume (nm ³)
3Y-TZP	3.606 (± 0.0007) ^{*)}	5.177 (± 0.0015) ^{*)}	1.0152	67.318×10^{-3}
3Y-TZP/30 vol % Mo	3.603 (± 0.0007)	5.174 (± 0.0019)	1.0154	67.167×10^{-3}
3Y-TZP/50 vol % Mo	3.601 (± 0.0007)	5.167 (± 0.0019)	1.0238	67.002×10^{-3}

^{*)} standard deviation within parentheses.

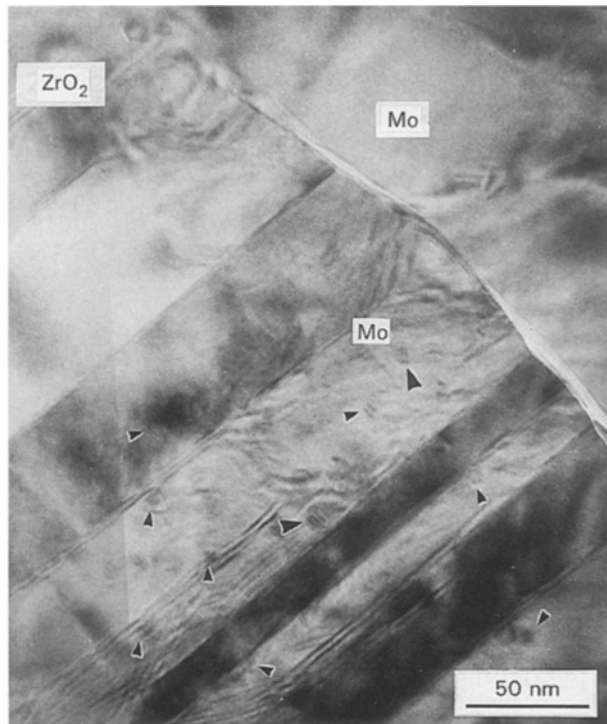


Figure 6 TEM image of the twins observed in the interface between ZrO_2 and Mo grain boundary for 3Y-TZP/40 vol % Mo composite.

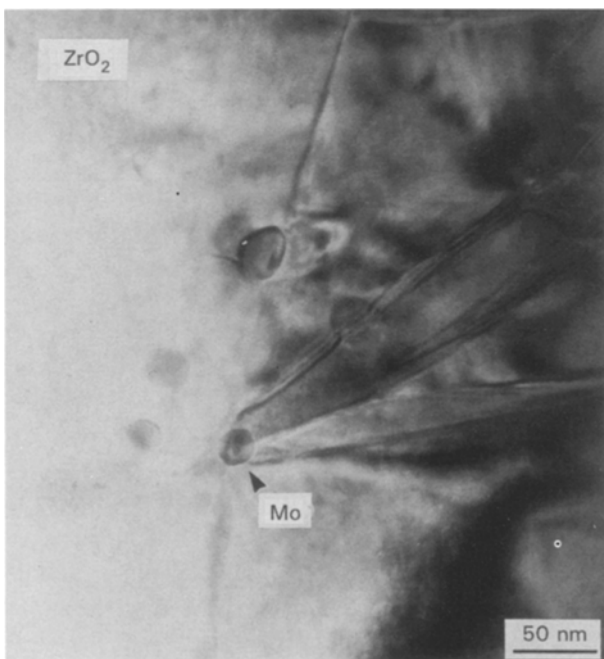


Figure 7 TEM image of the piled up dislocation lines observed around the nanometer sized Mo particle within the ZrO_2 grain.

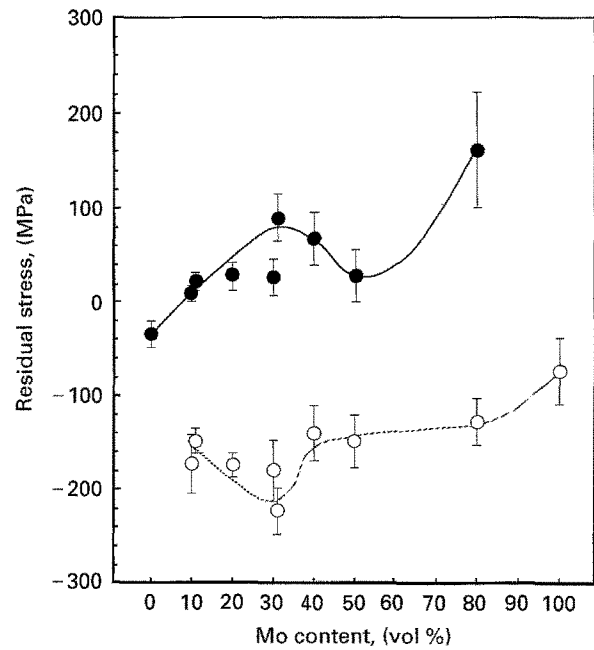


Figure 8 Variations of residual stress of both (●) ZrO_2 and (○) Mo phases with Mo content for 3Y-TZP/Mo composites.

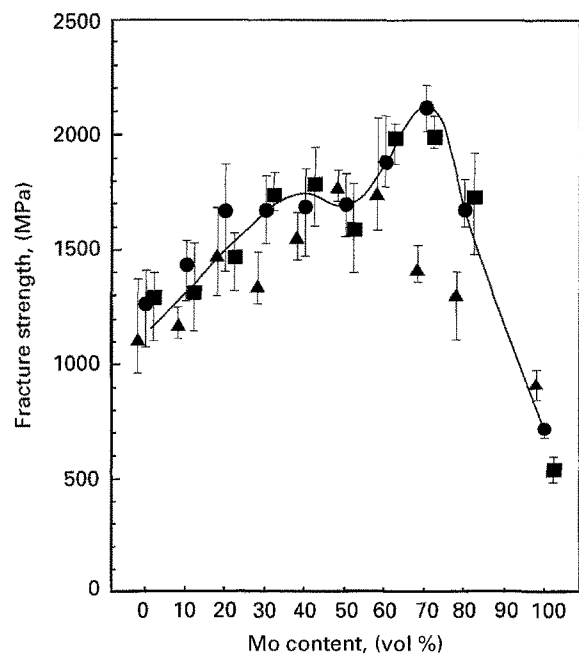


Figure 9 Variation of fracture strength with Mo content for 3Y-TZP/Mo composites. Hot pressed at (▲) 1400 °C, (○) 1500 °C and (■) 1600 °C.

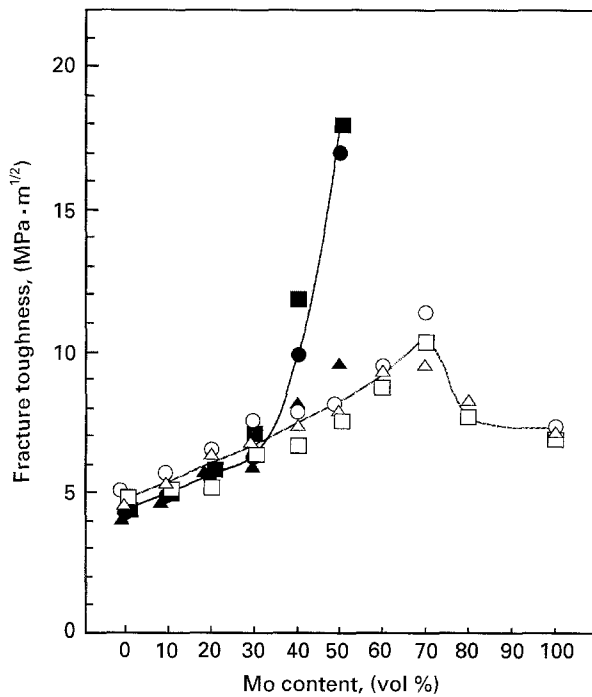


Figure 10 Variation of fracture toughness with Mo content for 3Y-TZP/Mo composites. Determined by IF method on samples hot pressed at (\blacktriangle) 1400 °C, (\bullet) 1500 °C and (\blacksquare) 1600 °C. Determined by SEVNB method on samples hot pressed at (\triangle) 1400 °C, (\circ) 1500 °C and (\square) 1600 °C.

Mo polycrystals resulting from the intragranular ZrO_2 dispersions. The second phenomenon concerns the stress induced phase transformation on the strengthening for Y-TZP ceramics. It has been determined that the retention of the tetragonal phase is critically governed by the grain size [1] and/or the internal strain or stress [25]. That is, reduction of the grain size and the internal residual stress are predicted to increase the critical stress that induces the tetragonal-to-monoclinic transformation. It has become apparent that the increase of the critical stress leads to augmentation of the strength of the Y-TZP ceramics [7]. As described above, these interactive contributions are considered to result in the improvement of the strength for the 3Y-TZP/Mo composites.

The dependence of the fracture toughness on the Mo content, which was both evaluated by the IF method and the SEVNB method, is shown in Fig. 10. In the IF method, the toughness was gradually improved with increasing Mo content up to 30 vol %. On the contrary, a notable increase of the toughness was achieved above 40 vol % Mo content. A maximum value of $18.0 \text{ MPa}\cdot\text{m}^{1/2}$ was obtained for the 3Y-TZP/50 vol % Mo composite hot-pressed at 1600 °C. In the range above 50 vol % Mo content, a crack could not be introduced by the Vickers indentation, which shows that a remarkable increase of the toughness was achieved. However, since the higher toughness value, above $10 \text{ MPa}\cdot\text{m}^{1/2}$, seems to be overestimated, various evaluation methods were investigated, such as the single-edge-precracked-beam (SEPB) method [26] and the chevron notch (CN) method [27]. In the case of the SEPB method, it was extremely difficult to introduce a pop-in precrack

arising from either a Vickers or a Knoop indent as a crack starter. Moreover, even in the CN method, a stable crack extension could not be obtained, although various notch angles (84° – 121.5°) were investigated. Consequently, the SEVNB method was selected as an improved evaluation technique. The required toughness can be accurately obtained by forming a sharper V-shaped notch with very small root curvature [23]. In this study, the specimens, having a V notch root radius around 10–15 μm , were subjected to the SEVNB test. In contrast to the IF method, the toughness increased continuously with increasing Mo content up to 70 vol % and exhibited a maximum value of $11.4 \text{ MPa}\cdot\text{m}^{1/2}$ for the 3Y-TZP/70 vol % Mo composite hot-pressed at 1400 °C. In the range above 80 vol % Mo, however, the toughness decreased to around $7 \text{ MPa}\cdot\text{m}^{1/2}$, despite the fact that a commercially available Mo plate exhibits a tensile plastic deformation of more than 30 % [21]. The reasons for the decrease of the toughness of the hot-pressed Mo polycrystals are not well understood, but the following possibilities are considered. First, the Mo polycrystals, hot-pressed at 1400–1600 °C, were composed of fine particle sizes from 3–10 μm , and exhibited a duplex microstructure, in which MoO_2 particles were dispersed within the Mo grains and at the grain boundaries. Second, an intergranular fracture mode was observed for all Mo polycrystals hot-pressed at 1400–1600 °C, due to the fine-grained microstructure and/or the existing impurities at the grain boundaries such as the MoO_2 phase. This intergranular fracture seemed to prevent the appearance of elongation ability of Mo and resulted in the lower toughness values in this study.

The volume fraction of the monoclinic phase in both polished and fractured surfaces, as a function of Mo content for the 3Y-TZP/0–80 vol % Mo composites, is shown in Fig. 11. In the polished surfaces,

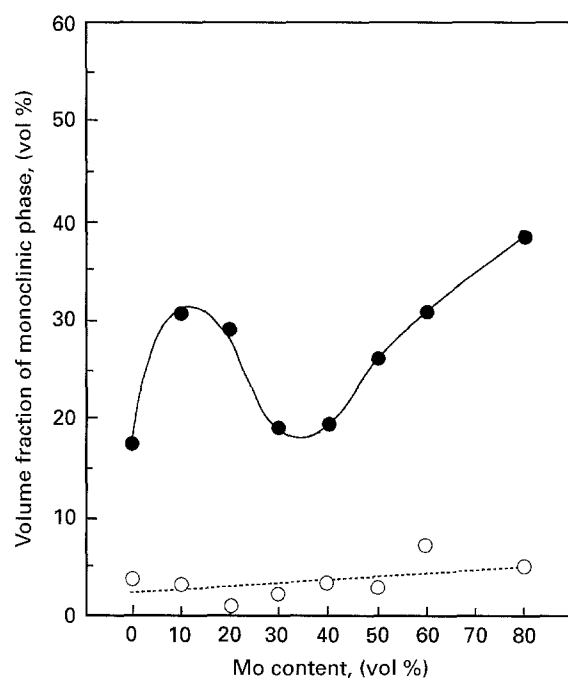


Figure 11 Variation of volume fraction of the monoclinic phase with Mo content in both (\circ) polished and (\bullet) fractured surfaces for 3Y-TZP/Mo composites hot-pressed at 1600 °C.

a slight increase of the monoclinic phase was observed in proportion to the Mo content, which were derived from the increase of the tensile residual stress in the ZrO_2 matrix. On the other hand, the volume fraction of the monoclinic phase in the fractured surface tended to increase overall for all Mo content values. However, especially in the range from 10–30 vol % Mo, a general decreasing tendency was observed. To understand the above variation behaviour, the phase stability of the tetragonal phase should be considered in conjunction with the accumulation state of the strain or the stress for the 3Y-TZP/Mo composites. Yoshimura [28] proposed that a strain accumulation, which leads to the nucleation of transformation, is required for the tetragonal-to-monoclinic transformation. Moreover, he pointed out that some defects such as dislocations and/or twins provide stress-sinks through interaction with applied external stresses. The influence of such stress-sinks on the stress induced phase transformation is thought to act as the restraint for the tetragonal-to-monoclinic transformation. This notion seems to be effective in interpreting our experimental results for the 3Y-TZP/Mo composites containing up to 40 vol % Mo content. As for the increase of the transformed monoclinic phase above 40 vol % Mo content, a fairly high tensile residual stress in the ZrO_2 grains resulted in the promotion of the tetragonal-to-monoclinic transformation.

With regard to the toughening, an additional mechanism is considered to act besides the stress induced phase transformation for the 3Y-TZP/Mo composites as compared to other TZP-based composite systems such as Y-TZP/ Al_2O_3 and Ce-TZP/ Al_2O_3 . In such systems, the toughness decreased with increasing Al_2O_3 content, which corresponds to the restraint in the tetragonal-to-monoclinic transformation [4]. On the other hand, 3Y-TZP/Mo composites exhibited a continuous improvement in toughness with increasing Mo content up to 70 vol % Mo. Nevertheless, the volume fraction of the monoclinic phase in the fractured surface decreased in the range from 10–30 vol % Mo content, which predicts a decrease in the toughness. These results revealed that the contribution of the stress-induced transformation toughening is not a dominant factor for the 3Y-TZP/Mo composites in the region of high toughness.

Fig. 12 shows the representative crack propagation behaviour around the Vickers indentation for the 3Y-TZP/Mo composites containing 20 and 40 vol % Mo content, which was hot-pressed at 1600 °C. In less than 20 vol % Mo content, cracks propagated in a straight direction with small deviations around Mo particles, which corresponded to the lower toughness. On the contrary, with increasing Mo content above 40 vol % Mo, cracks were deflected and bridged by the elongated Mo polycrystals at the ZrO_2 grain boundaries. Furthermore, as indicated by the arrows, it was occasionally observed that the crack propagated through the elongated Mo polycrystals, which corresponded to the higher toughness. These interactions between the crack tip and the metal phase were determined to result in the stress shielding effect, which related to the relaxation of stress intensity deriving

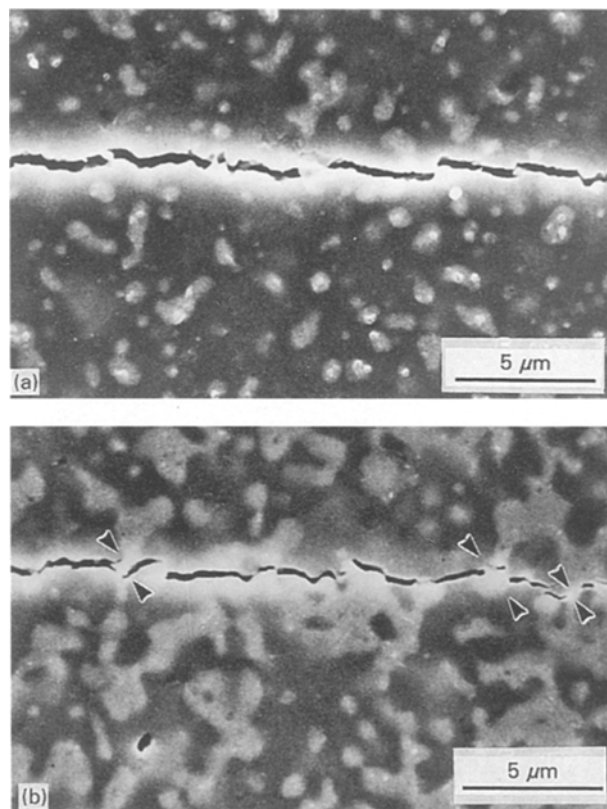


Figure 12 SEM photographs of crack propagation behaviour around the Vickers indentation for 3Y-TZP/Mo composites containing 20 vol % (a) and 40 vol % (b) Mo.

from blunting and/or bridging of the crack tip by the elongated Mo polycrystals. Consequently, this caused a substantial increase in the toughness for 3Y-TZP/Mo composites.

The elastic modulus and Vickers hardness, as a function of Mo content for the 3Y-TZP/0–100 vol % Mo composites, are shown in Figs 13 and 14, respectively. In each figure, dotted lines represent the calculated values by the linear rule of mixtures using the experimental data of the monolithic 3Y-TZP and the Mo polycrystal for the initial values of 0 and 100 vol % Mo, respectively. On the whole, the variations of elastic modulus and Vickers hardness with Mo content were approximately in good agreement with the predicted changes by the linear rule of mixtures. In the case of the Vickers hardness, however, it was recognized that the hardness depended on both the hot-pressing temperature and Mo content. As for the influence of the hot-pressing temperature, a slight decrease in the hardness was observed with increasing hot-pressing temperature for both monolithic 3Y-TZP and 3Y-TZP/Mo composites at all Mo contents. These decreases in the hardness are thought to be attributed to the existence of the coalesced and elongated Mo polycrystals at the ZrO_2 grain boundaries. With regard to the variation of hardness with Mo content, it was noticed that hardening occurred in the range from 60–80 vol % Mo content. This hardening behaviour is believed to be responsible for the modification of Mo polycrystals associated with the novel intragranular microstructure. That is, the mobility of the dislocation of the Mo would be inhibited and/or

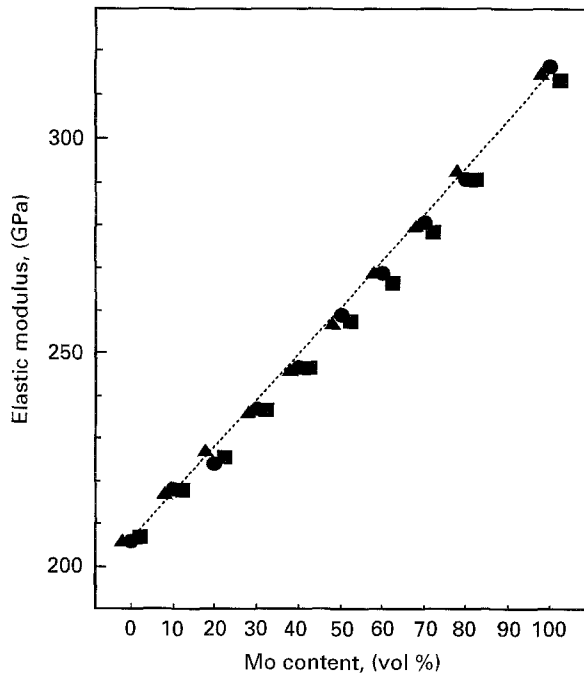


Figure 13 Variation of elastic modulus with Mo content for 3Y-TZP/Mo composites containing 0 to 100 vol % Mo. Samples hot pressed at (▲) 1400°C, (●) 1500°C and (■) 1600°C.

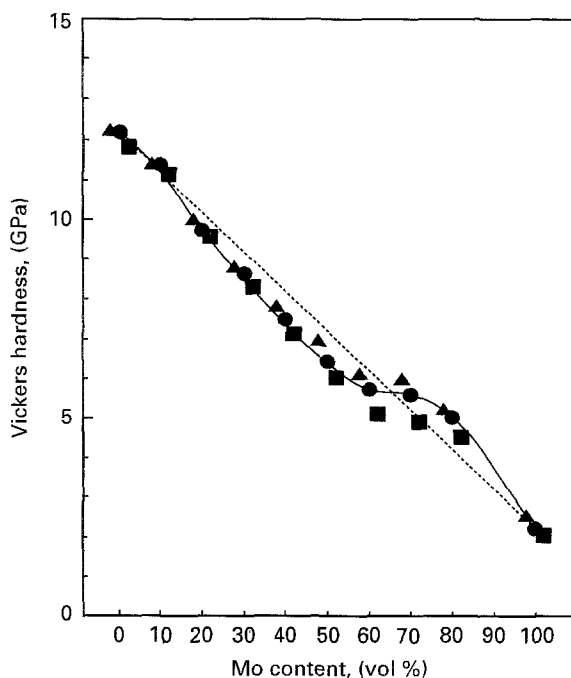


Figure 14 Variation of Vickers hardness with Mo content for 3Y-TZP/Mo composites containing 0 to 100 vol % Mo. Samples hot pressed at (▲) 1400°C, (●) 1500°C and (■) 1600°C.

pinned by the fine-grained ZrO_2 particles within the Mo grains, which is a similar mechanism to precipitation hardening.

4. Conclusions

To overcome the strength-toughness tradeoff relation in Y-TZP based composite systems, we investigated 3Y-TZP based nanocomposites incorporating a ductile refractory metal (Mo). The microstructures for the 3Y-TZP/0-100 vol % Mo composites and the

relationship between their mechanical properties were examined. The results are summarized as follows:

(I) 3Y-TZP/10-80 vol % Mo composites hot-pressed at 1400-1600°C were composed of only ZrO_2 and Mo. No crystalline reaction phases were detected. The ZrO_2 matrix in these composites consisted of primarily the tetragonal phase and a small amount of the monoclinic phase. There were no traces of the cubic phase.

(II) For less than 30 vol % Mo content, submicron sized Mo particles were dispersed at the grain boundaries of fine-grained/submicron sized ZrO_2 grains. Furthermore, fine-grained Mo particles were partly trapped within the ZrO_2 grains. On the other hand, in the above 40 vol % Mo content samples, elongated Mo polycrystals were gradually formed at the ZrO_2 grain boundaries. In addition, they possessed a novel interpenetrated intragranular nanostructure, in which either nanometer sized Mo or equivalent sized ZrO_2 particles were located within the ZrO_2 grains or Mo grains, respectively. Finally, for above 60 vol % Mo content, a linked structure of Mo layers was produced.

(III) The fracture strength and toughness were greatly enhanced simultaneously with increasing Mo content. This breaks through the strength-toughness tradeoff relation, although the Vickers hardness decreased with increasing Mo content. They exhibited a maximum strength of 2100 MPa and a toughness of $11.4 \text{ MPa} \cdot \text{m}^{1/2}$ (SEVNB) for the composite containing 70 vol % Mo. The appearance of the simultaneous improvements in strength and toughness was determined to be the result of a decrease in flaw size, associated with the interpenetrated intragranular nanostructure, and a stress shielding effect created in the crack tip by the elongated Mo polycrystals bridging the crack tip in addition to the stress induced phase transformation.

References

1. T. K. GUPTA, F. F. LANGE and J. H. BECHTOLD, *J. Mater. Sci.* **13** (1978) 1464.
2. K. MASAKI, *J. Amer. Ceram. Soc.* **69** (1986) 638.
3. K. TSUKUMA and M. SHIMADA, *J. Mater. Sci.* **20** (1985) 1178.
4. K. TSUKUMA, K. UEDA and M. SHIMADA, *J. Amer. Ceram. Soc.* **68** (1985) C5.
5. R. SHIKATA, Y. URATA, T. SHIONO and T. NISHIKAWA, *J. Jpn. Soc. Powder and Powder Metall.* **37** (1990) 357.
6. K. TSUKUMA, T. TAKAHATA and M. SHIOMI, in *Advances in Ceramics, 24, Science and Technology of Zirconia III*. (The American Ceramic Society, Westerville, OH, 1988) pp. 721-28.
7. M. V. SWAIN and L. R. F. ROSE, *J. Amer. Ceram. Soc.* **69** (1986) 511.
8. P. HING, *Sci. Ceram.* **10** (1980) 521.
9. C. O. McHUGH, T. J. WHALEN and M. HUMENIK, Jr., *J. Amer. Ceram. Soc.* **49** (1966) 486.
10. D. T. RANKIN, J. J. STIGLICH, D. R. PETRAK and R. RUH, *ibid.* **54** (1971) 277.
11. Y. NAERHEIM, *Powder Metall. Int.* **18** (1986) 158.
12. S. A. CHO, M. PUERTA, B. COLS and J. C. OHEP, *ibid.* **12** (1980) 192.
13. E. BREVAL, G. DODDS and C. G. PANTANO, *Mat. Res. Bull.* **20** (1985) 1191.

14. K. NIIHARA, A. NAKAHIRA, T. UCHIYAMA and T. HIRAI, in "Fracture Mechanics of Ceramics 7", Edited by R. C. Bradt, A. G. Evans, D. P. H. Hasselman and F. F. Lange (Plenum Press, New York, 1986) p. 103.
15. K. NIIHARA, *J. Ceram. Soc. Jpn.* **99** (1991) 974.
16. M. NAWA, T. SEKINO and K. NIIHARA, *J. Mater. Sci.* **29** (1994) 3185.
17. M. NAWA, K. YAMAZAKI, T. SEKINO and K. NIIHARA, *Mater. Lett.* **20** (1994) 299.
18. R. C. GARVIE and P. S. NICHOLSON, *J. Amer. Ceram. Soc.* **55** (1972) 303.
19. H. TORAYA, M. YOSHIMURA and S. SOMIYA, *ibid.* **67** (1984) C-119.
20. K. TANAKA, N. MINE, R. SHIKATA and Y. NISHIKAWA, in Proceedings of the 27th Symposium on X-ray Studies on Mechanical Behaviour of Materials (J. Mat. Sci. Jpn), (Plenum, Kyoto, 1990) p. 43.
21. C. S. SMITHELLS, "Metals Reference Book vol. 3", (Butterworths, London, 1967) 917.
22. D. B. MARSHALL and A. G. EVANS, *J. Amer. Ceram. Soc.* **64** (1981) C-182.
23. H. AWAJI, T. WATANABE and Y. SAKAIDA, *Ceram. Int.* **18** (1992) 11.
24. J. E. SRAWLEY, *Int. J. Fract.* **12** (1976) 475.
25. F. F. LANGE, *J. Mater. Sci.* **17** (1982) 240.
26. T. NOSE and T. FUJII, *J. Amer. Ceram. Soc.* **71** (1988) 328.
27. D. MUNZ, R. T. BUBSEY and J. L. SHANNON Jr., *ibid.* **63** (1980) 300.
28. M. YOSHIMURA, *Ceram. Bull.* **67** (1988) 1950.

*Received 15 June 1995
and accepted 20 November 1995.*